Inorganic Chemistry

Article

pubs.acs.org/IC

Solvent-Dependent Pyranopterin Cyclization in Molybdenum Cofactor Model Complexes

Benjamin R. Williams, Douglas Gisewhite, Anna Kalinsky, Alisha Esmail, and Sharon J. Nieter Burgmayer*

Department of Chemistry, Bryn Mawr College, Bryn Mawr, Pennsylvania 19010, United States

Supporting Information

ABSTRACT: The conserved pterin dithiolene ligand that coordinates molybdenum (Mo) in the cofactor (Moco) of mononuclear Mo enzymes can exist in both a tricyclic pyranopterin dithiolene form and as a bicyclic pterin−dithiolene form as observed in protein crystal structures of several bacterial molybdoenzymes. Interconversion between the tricyclic and bicyclic forms via pyran scission and cyclization has been hypothesized to play a role in the catalytic mechanism of Moco. Therefore, understanding the interconversion between the tricyclic and bicyclic forms, a type of ring−chain tautomerism, is an important aspect of study to understand its role in catalysis. In this study, equilibrium constants (K_{eq}) as well as enthalpy, entropy, and free energy values are obtained for pyran ring tautomerism exhibited by two Moco model complexes, namely, $(Et_4N)[Tp^*Mo(O)(S_2BMOPP)]$ (**1**) and $(Et_4N)[Tp^*Mo(O)(S_2PEOPP)]$ (**2**), as a solvent-dependent equilibrium process. K_{eq} values obtained from ^1H NMR data in seven deuterated solvents show a correlation between solvent polarity and tautomer form, where solvents with higher polarity parameters favor the pyran form.

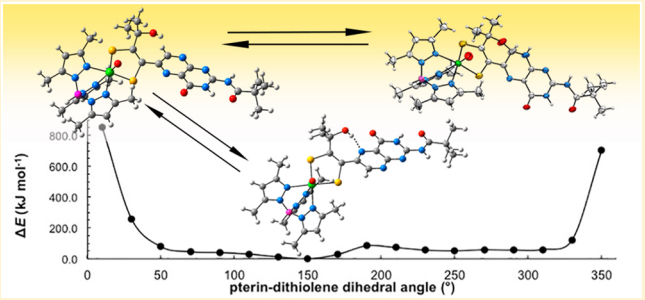

INTRODUCTION

Mononuclear molybdenum (Mo) and tungsten (W) enzymes form a diverse group of enzymes whose roles in biological metabolic and catabolic processes primarily involve transfer of oxygen atoms in simple reactions having critical importance to the health of the organism. These metalloenzymes have at their active site a unique and structurally complex cofactor that contains either one or two conserved pyranopterin dithiolene ligands commonly known as "molybdopterin" (MPT).[1] The chemical structure of MPT was largely gleaned from chemical degradation studies by Rajagopalan et al. and has been defined in more detail in protein crystal structures.[2,3] These X-ray structures depict MPT in the majority of molybdenum enzymes as a triheterocyclic dithiolate chelate (Figure 1a) containing a pterin moiety and a pyran ring, both attached to a dithiolene group that serves as the chelating unit coordinated to the Mo or W center.

Despite decades of research in molybdoenzymes and model studies of its cofactor Moco, the connection between the highly conserved ligand MPT in Moco and its catalytic function remains obscure.[5,6] In part, our lack of knowledge regarding the precise role of MPT in Moco has been limited by its in vitro instability outside of the protein matrix. Yet it is well understood that MPT coordination to Mo in Moco is required for proper enzymatic function, highlighting the importance of MPT as a vital part of Moco.[2,7] This fact has spurred a growing interest in elucidating the role MPT plays during catalysis. Since the pterin system is able to achieve different oxidation states through sequential $2e^-/2H^+$ redox processes, it has been speculated that it might participate with the dithiolene in modulating Mo redox potentials.[5,8−13] Evidence that pterin may indeed play a role in tuning catalysis emerged from a detailed analysis of pyranopterin conformations in Mo and W protein crystal structures.[6] This study revealed a correlation between pterin conformation and enzyme function where the pterin conformation was interpreted as resulting from different oxidation states.[6]

The pyran ring joining the dithiolene chelate to the pterin in MPT may also have a part in tuning catalysis. Some have speculated that the pyran ring has the capacity to undergo ring scission and produce a bicyclic "open" form as shown in Figure 1b.[6,14] This expectation was initially based on reactivity that was documented in the first report of a synthetic pyranopterin.[15,16] Pyran ring scission of MPT would disrupt the electronic environment felt by the dithiolene as the tetrahydro-pyrazine ring (Figure 1a) becomes the 5,6-dihydro system (Figure 1b). Reinforcing this notion that pyran ring scission may occur and have a specific function, two protein crystal structures of bis-MPT sites in bacterial molybdoenzymes exhibit the Moco site as possessing two MPT ligands in different forms, one a tricyclic pyranopterin-dithiolene and one a bicyclic, open pterin−dithiolene, thereby providing structural evidence that reversible pyran cyclization dynamics may be achievable within the active site.[17,18]

Received: March 7, 2015
Published: May 5, 2015

ACS Publications © 2015 American Chemical Society

DOI: 10.1021/acs.inorgchem.5b00532
Inorg. Chem. 2015, 54, 8214−8222

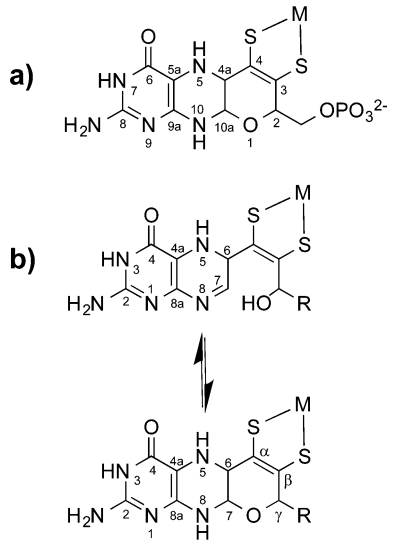

Figure 1. (a) Chemical structure and IUPAC numbering of MPT in the tricyclic pyranopterin form and (b) pyran cyclization equilibrium with the numbering system used in this paper.[4] Note that, although the pterin IUPAC numbering system changes upon cyclization, the uncyclized numbering system (in (b), upper structure) will be used throughout this paper for simplicity. M = Mo or W; R = phosphate or a dinucleotide.

Reports of pyran formation and scission in chemical models of Moco are limited. Joule et al. achieved pyran cyclization in their quinoxaline- and pteridine-containing Moco models after alkylation and subsequent pyrazine reduction.[19,20] In a study not directed at modeling Moco, Pfleiderer and Soyka also observed pyran scission in a simple pteridine system.[15,16] We subsequently investigated this system in terms of its redox behavior and kinetics under various reductive and oxidative conditions and concluded that the pyran ring protected the reduced pyranopterin from oxidation to neopterin, which requires scission of the pyran ring to occur.[21] In a recent communication, we reported the synthesis of the first Moco model complex containing a pyranopterin dithiolene ligand bound to Mo, $(Et_4N)[Tp^*Mo(O)(S_2BMOPP)]$ (**1**), where Tp* = tris(3,5-dimethylpyrazolyl)hydroborate, and described our initial observations regarding the ability of this model to undergo reversible, solvent-dependent pyran cyclization.[22] Here we report a new model, $(Et_4N)[Tp^*Mo(O)(S_2PEOPP)]$ (**2**), and detailed investigations of the ring−chain tautomerism involving the pyranopterin in both **1** and **2** (PEOPP = 6-(3-pentynyl-2-ethyl-2-ol)-2-pivaloyl pterin). The chemical structures of both complexes, as well as the pyran cyclization equilibrium they exhibit, are depicted in Figure 2. The incorporation of model **2** in this study was intended to probe the role of sterics in the observed pyran tautomerism. The equilibrium between the open form and the cyclized pyrano form of the pterin−dithiolene chelates S_2BMOPP and S_2PEOPP was studied by ^{1}H NMR and measured in seven solvents to yield equilibrium constants (K_{eq}) and thermodynamic parameters (ΔH, ΔS, and ΔG) for pyran cyclization in **1** and **2**. The set of K_{eq} values reveal that the pyran form is favored with increasing solvent polarity, based on solvent dielectric constant, whereas the open chain, pterin−dithiolene form predominates in low polarity (low dielectric) solvents.

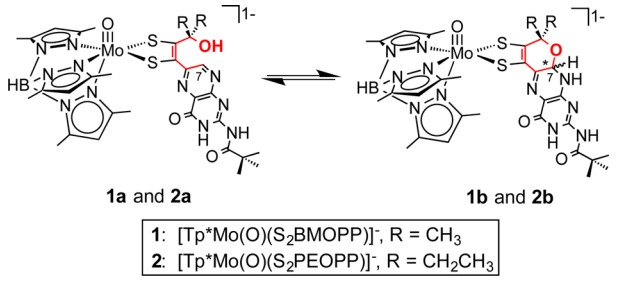

Figure 2. Equilibrium between the open chain forms **1a** and **2a** and the cyclized pyran forms **1b** and **2b**. The pyran ring that is involved in the tautomerism is highlighted in red. Cyclization causes the formation of two diastereomers, forming either the *R* or *S* isomer at the chiral carbon C7 marked by an asterisk.

EXPERIMENTAL SECTION

Materials and Methods. The syntheses of $(Et_4N)[Tp^*Mo(S)(S_4)]$, 2-pivaloyl-6-chloropterin, and $(Et_4N)[Tp^*Mo(O)(S_2BMOPP)]$ (**1**) were performed using previously published procedures.[22,23] All other reagents, chemicals, and deuterated solvents were purchased from Sigma-Aldrich and used as received. All solvents for syntheses were purchased from Pharmco-AAPER and were deaerated with N_2 gas over activated neutral alumina before use. Electrospray ionization mass spectrometry (ESI-MS) analyses were performed using a Waters Micromass-ZQ mass spectrometer at Bryn Mawr College via infusion of samples as acetonitrile solutions. All NMR experiments were performed on a Bruker 400 MHz FT-NMR. Infrared spectra were obtained using a PerkinElmer Frontier FT-IR on samples prepared as KBr pellets.

6-(3-Pentynyl-2-ethyl-2-ol)-2-pivaloyl Pterin. 2-Pivaloyl-6-chloropterin (1.0046 g, 3.5662 mmol), CuI_2 (0.1039 g, 0.5456 mmol), $Pd(OAc)_2$ (0.1009 g, 0.4494 mmol), and 1,1′-bis-(diphenylphosphino) ferrocene (BDPF) (0.2512 g, 0.4531 mmol) were combined in 30 mL of acetonitrile and magnetically stirred for 10 min, after which 3-ethyl-1-pentyn-3-ol (2.6 g, 23 mmol) and triethylamine (3.6 g, 35.8 mmol) were added via syringe under N_2 gas using standard Schlenk techniques. The resulting brown solution was stirred for 4 h at 42.5 °C, then diluted with dichloromethane (30 mL), chilled for 30 min at 0 °C, and then filtered. Diethyl ether (20 mL) was added to the filtrate. The resulting precipitate was subsequently filtered, washed with water (20 mL), and dried under vacuum to produce PEOPP (1.2562 g, 99.0%) as a tan solid. ^{1}H NMR ($CDCl_3$) δ: 8.87 (1H, s), 1.85 (4H, q), 1.37 (9H, s), 1.15 (6H, t). FT-IR (KBr pellet, cm^{-1}): ν(O−H) 3342, ν(N−H) 3246, 3173, 3112, ν(C≡C) 2221, ν(C═O) 1682, 1612, ν(C═N) 1556, 1478, 1443. Anal. Calcd (%) for $C_{18.5}H_{24}N_5O_3Cl$, (PEOPP·1/2 CH_2Cl_2): C, 55.57; H, 6.049. Found: C, 55.61; H, 5.69.

$(Et_4N)[Tp^*Mo(O)(S_2PEOPP)]$ (2). Under N_2 gas, $(Et_4N)[Tp^*Mo(S)S_4]$ (0.2004 g, 0.2926 mmol) and PEOPP (0.1020 g, 0.2854 mmol) were magnetically stirred in wet acetonitrile (8 mL, 1% H_2O v/v) to produce a brown solution that was heated for 2 h at 63 °C. Addition of diethyl ether precipitated a reddish-brown solid that was subsequently filtered and dried under vacuum, yielding (Et_4N)-$[Tp^*Mo(S)(S_2PEOPP)]$, ESI-MS: $[M^-]$ = 848 m/z, $[M + 2TEA^+]$ = 1108 m/z (TEA = tetraethylammonium). After redissolving (Et_4N)-$[Tp^*Mo(S)(S_2PEOPP)]$ in wet acetonitrile (8 mL, 1% H_2O v/v), tributylphosphine (0.20 g, 1.0 mmol) was added dropwise. The brown solution was stirred for 2.5 h at room temperature. Addition of diethyl ether caused precipitation of a brown solid that was filtered and dried under vacuum to produce **2** (0.0883 g, 60%). ^{1}H NMR ($CDCl_3$, ppm) δ: 11.63 (2H, s), 9.40 (1H, s), 5.94 (1H, s), 5.88 (1H, s), 5.85 (1H, s), 5.43 (1H, s), 2.76 (4H, s), 2.64 (3H, s), 2.43 (3H, s), 2.23 (3H, s), 2.16 (3H, s), 2.14 (3H, s), 1.42 (6H, q), 1.38 (9H, s), 1.26 (3H, s). FT-IR (KBr pellet, cm^{-1}): 3428 ν(O−H), 3250 ν(N−H), 2546 ν(B−H), 1657 ν(C═O), 1613, 1544 ν(C═N), 1479, 1449, 928 (Mo≡O). ESI-MS: $[M^-]$ = 832 m/z, $[M + 2TEA^+]$ = 1092 m/z.

DOI: 10.1021/acs.inorgchem.5b00532
Inorg. Chem. 2015, 54, 8214−8222

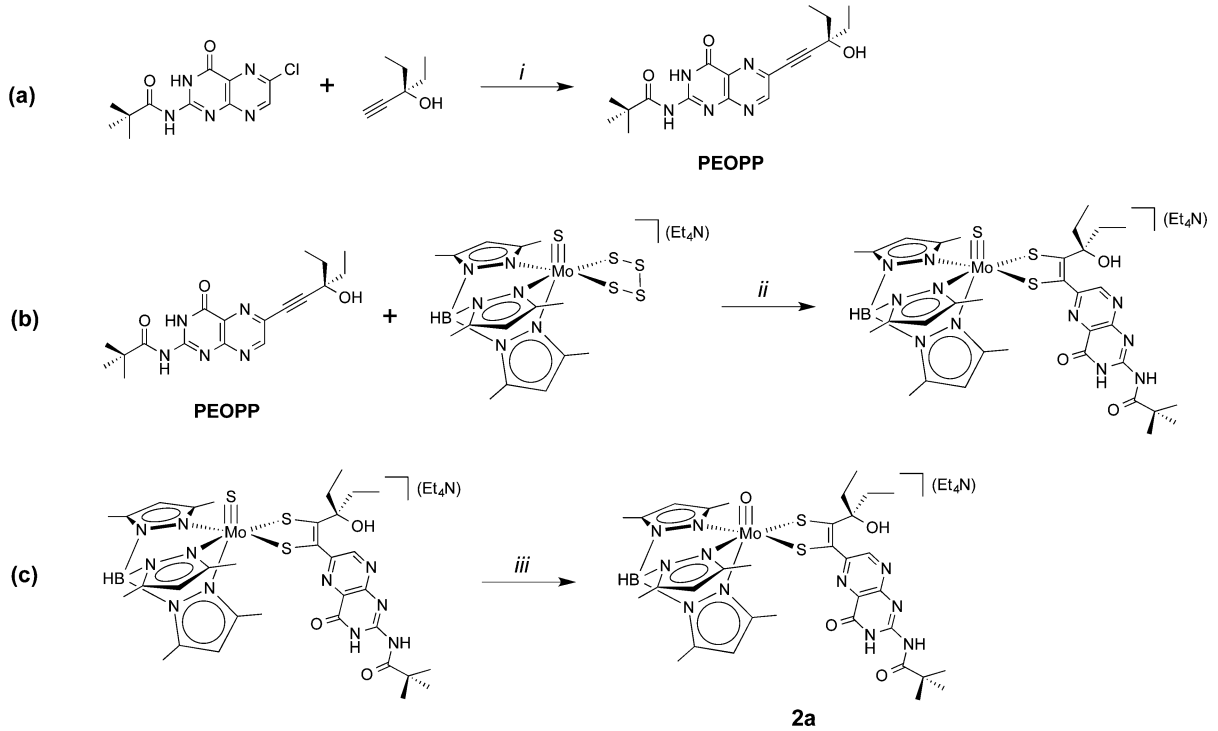

Figure 3. (a) PEOPP alkyne synthesis; (b) reaction of PEOPP and $(Et_4N)[Tp^*Mo(S)(S_4)]$ to produce $(Et_4N)[Tp^*Mo(S)(S_2PEOPP)]$; (c) hydrolysis of the terminal sulfido ligand on Mo. (i) CuI_2, $Pd(OAc)_2$, BDPF, Et_3N, MeCN at 42.5 °C; (ii) 1% H_2O in MeCN, 2 h at 63 °C; (iii) 5 equiv of PBu_3, 1% H_2O in MeCN, 2.5 h at 25 °C.

Computational Methods. Geometry optimization and energy calculations were performed at the density functional level of theory (DFT) using the Gaussian09 collection of software.[24] Input files were created and manipulated using Gaussview. Calculations used the B3LYP hybrid functional and applied the Stuttgart/Dresden (SDD) basis set and effective core potential to Mo and the 6-31G* basis set to all other atoms in the molecule. Pterin rotation calculations were performed starting with the optimized structure of **1a** but with varying pterin−dithiolene dihedral angles while maintaining the optimized structure for the remaining complex.

RESULTS

Synthesis and Characterization of 2. The overall synthetic pathway for **2** is outlined in Figure 3. In a previous report,[23] we established that Mo complexes containing pterin dithiolenes can be achieved by the reaction of a pterinyl alkyne with a molybdenum tetrasulfide complex. The synthesis of **2** employs this same strategy as shown in Figure 3 using the pterinyl alkyne PEOPP. The Sonogashira cross-coupling reaction between 2-pivaloyl-6-chloropterin and 3-ethyl-1-pentyn-3-ol produces the tan-colored PEOPP alkyne in high yield (Figure 3a). The subsequent reaction of PEOPP and $(Et_4N)[Tp^*Mo(S)(S_4)]$ produces $(Et_4N)[Tp^*Mo(S)(S_2PEOPP)]$ (Figure 3b). Ethyl substitution on the alkyne creates steric resistance to coupling of the alkyne and tetrasulfide; hence, the reaction requires a higher temperature to achieve dithiolene formation. Subsequent hydrolysis of the sulfido ligand is facilitated by excess (5 equiv) tributylphosphine in the presence of water and oxygen (Figure 3c). The role of phosphine is presumed to be labilization of the Mo≡S bond toward hydrolysis. Addition of O_2 in the reaction flask was found to expedite this hydrolysis reaction, but the details regarding this reaction are not yet known. Care is required since O_2 also oxidizes the Mo(IV) metal to Mo(V) at longer reaction times.

Equilibrium Measurements. ^{1}H NMR spectroscopy has been documented as a convenient method to obtain K_{eq} constants in systems exhibiting ring−chain equilibria, and this approach was used to determine K_{eq} values for **1** and **2**.[25−27] In the current study, equilibrium experiments were performed in seven deuterated solvents to study how the solvent environment affected the equilibrium between the cyclized, pyranopterin, and open pterin forms of complexes **1** and **2**. K_{eq} constants were calculated using the integrations of pertinent resonance signals corresponding to the open or pyran forms. Selected solvents included chlorinated solvents (chloroform-*d* and dichloromethane-d_2) as well as polar aprotic solvents (dimethyl sulfoxide-d_6 (DMSO-d_6), *N*,*N*-dimethylformamide-d_7 (DMF-d_7), acetonitrile-d_3, acetone-d_6, and tetrahydrofuran-d_8 (THF-d_8)). Polar protic solvents such as methanol-d_4 were avoided since ^{1}H NMR spectra of **1** and **2** in these solvents typically have broadened signals that complicate the acquisition of integration data.

Signals utilized for integration data were selected based on ^{13}C and HSQC NMR experiments (data not shown) and are shown in Figure 4 for **1** in chloroform-*d* and acetonitrile-d_3 and in all other deuterated solvents in Supporting Information, Figure S1 for **1** and in Supporting Information, Figure S2 for **2**. The integration of the resonance at ∼9.0−9.4 ppm corresponding to the pyrazine proton H7 was used as a measure of the relative amount of the uncyclized, open forms **1a** and **2a**. During cyclization to the pyrano forms **1b** and **2b**, H7 remains bound to carbon C7, whose tetrahedral character now produces a more shielded environment causing the H7 resonance to shift upfield between 5.8−6.0 ppm in all solvents; pyranopterin ^{1}H and ^{13}C NMR data from the literature

DOI: 10.1021/acs.inorgchem.5b00532
Inorg. Chem. 2015, 54, 8214−8222

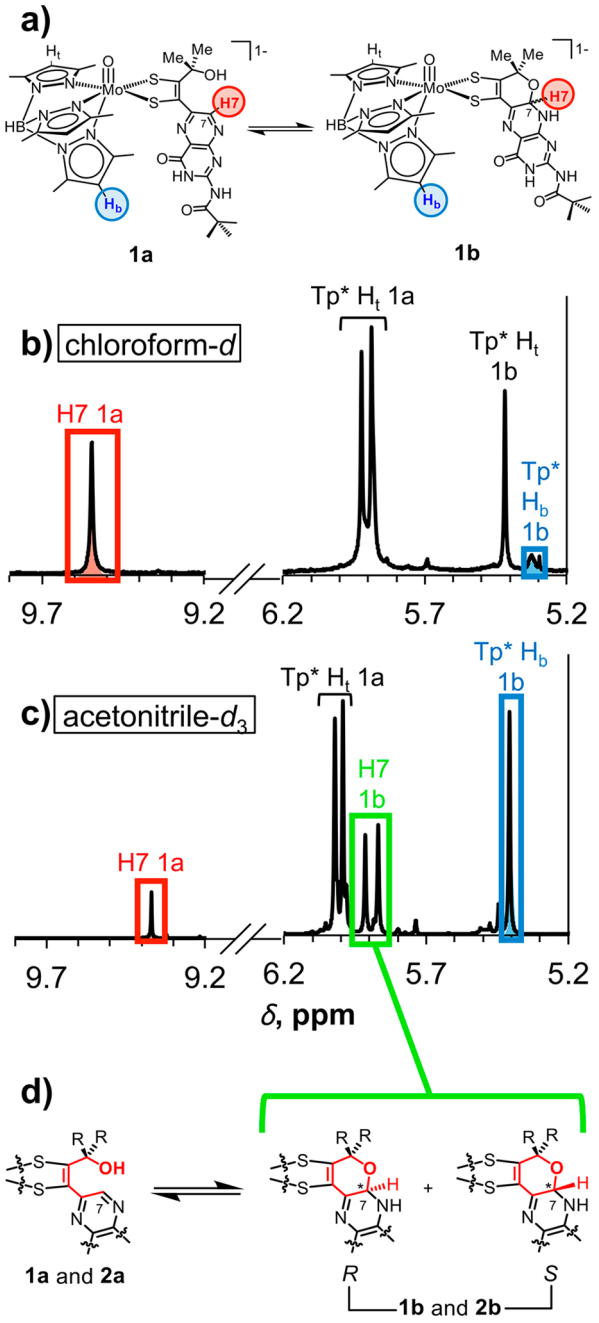

Figure 4. (a) Structures of **1a** and **1b** highlighting corresponding protons used for integration data from ^{1}H NMR spectra in (b) chloroform-*d* and (c) acetonitrile-d_3; (d) equilibrium between the open form **1a** or **2a** and the two *R* and *S* diastereomers of the pyran forms **1b** and **2b**; two signals in the ^{1}H NMR spectrum (highlighted in green in acetonitrile-d_3) are for H7 in the pyran form, each corresponding to either the *R* or *S* isomer.

corroborate this assignment.[15,28,29] Two signals are observed for H7 in the pyrano forms **1b** and **2b** since C7 becomes a chiral center upon cyclization and may form either the *R* or *S* enantiomer as observed from crystal structures of **1** (Figure 4d).[22] As a result, two separate signals are found to correspond to the proton in both enantiomers. Although the H7 resonance for **1b** in the pyrano form is isolated from any other signals in the ^{1}H NMR spectrum when obtained in acetonitrile-d_3, DMF-d_7, and DMSO-d_6, in the remaining solvents, H7 signals overlap with neighboring resonances corresponding to Tp* pyrazole protons, which complicates integration data. To circumvent this problem, integration data for the pyran form in both **1** and **2** were acquired from the proton signals corresponding to the bottom Tp* central pyrazole proton (blue H_b in Figure 4a, Supporting Information, Figures S1a and S2a). Two signals for Tp* H_b corresponding to the *R* and *S* enantiomers are observed in all solvents except acetonitrile-d_3 for **1b**, in which case these signals converge into one peak. Integrations of these two signals were summed to give the total amount of cyclized pyranopterin. We note that no additional resonances for other dihydropyranopterin tautomers other than the 7,8-dihydropyranopterin form of **1b** and **2b** (Figure 4a, right) were observed.

K_{eq} values obtained from ^{1}H NMR data are listed in Table 1 for complexes **1** and **2**. Since sterically bulky substituents near the site of tautomerism tend to push the equilibrium to the cyclized form,[26,27] it was thought that the additional steric bulk imposed on the system by the ethyl groups in **2** versus the methyl groups in **1** might cause **2** to have larger K_{eq} values. However, examination of the data seems to show this is not the case: all K_{eq} values for **2**, with exception of that for DMSO-d_6, are similar in magnitude to those for **1**.

Table 1. Pyran Cyclization Equilibrium Constants[a] for 1 and 2 in Various Deuterated Solvents Correlated with Solvent Dielectric Constants (ε)

solvent	K_{eq} (**1**)	K_{eq} (**2**)	ε
DMSO-d_6	14(2)	8(3)	46.7
DMF-d_7	6.9(7)	n/a[b]	36.7
acetonitrile-d_3	6.1(8)	5(1)	37.5
acetone-d_6	2.3(4)	2.0(6)	20.7
THF-d_8	1.6(2)	1.5(1)	7.58
dichloromethane-d_2	1.2(2)	1.8(4)	8.93
chloroform-*d*	0.41(5)	0.5(2)	4.81

[a] K_{eq} = [**1b**]/[**1a**] or K_{eq} = [**2b**]/[**2a**]. [b] Integration data not acquired due to convolution of signals in the ^{1}H NMR spectrum.

Because K_{eq} values in both **1** and **2** vary with solvent, we attempted to correlate physical solvent parameters with K_{eq} data to understand which solvent effects govern the equilibrium between pyranopterin−dithiolene and open chain pterin−dithiolene. Plotting solvent dielectric constant versus K_{eq} (Figure 5) shows that K_{eq} increases as the solvent dielectric constant increases. Solvent dipole moment, the empirical Kosower's *Z* constants,[30] and the empirical Kamlet−Taft hydrogen bond acceptor basicity scale (β_{KT})[31,32] provided

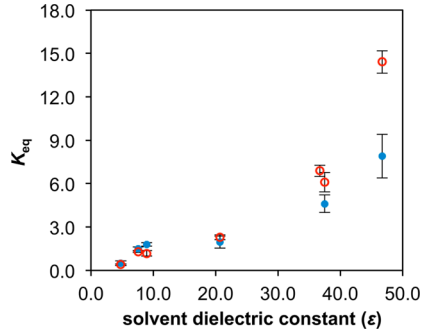

Figure 5. Plot of K_{eq} values versus solvent dielectric constant for **1** (red ○) and **2** (blue ●).

DOI: 10.1021/acs.inorgchem.5b00532
Inorg. Chem. 2015, 54, 8214−8222

similar trends as dielectric constants but with poorer correlations (Supporting Information, Figure S3).

The trend shown in Figure 5 was compared to studies on ring−chain tautomerism in imine- and carbonyl-containing organic molecules. While the majority of ring−chain tautomerism studies find that increasing solvent polarity generally favors the chain (open) form,[26,33−37] a few studies exist whose results mirror ours where polar solvents favor the cyclized form.[38−40] However, these studies agree that polar solvents preferentially solubilize and stabilize the more polar form of the molecule undergoing ring−chain tautomerism.[27,34,38] On the basis of the K_{eq} data in Table 1, it may be inferred that the pyran form of **1** and **2** is more polar than the open form.

Other factors contributing to the observed trend in Figure 5 can be considered. One is that polar solvents could stabilize a charged intermediate between the open and pyran forms, enhancing the thermodynamic accessibility of the pyran form. Another factor is the ability of more polar solvents to act as Brønsted-Lowry acids/bases, aiding proton migration from the hydroxyl oxygen in the open form (**1a**, **2a**) to N8 in the pyran form (**1b**, **2b**).[26] It has been argued that hydrogen bonds between polar, aprotic solvents and the −OH group of hydroxyl-containing imines stabilize the open form in those molecules.[26,33] Solvent formation of hydrogen bonds will certainly occur with both the pyranopterin tautomers **1b** and **2b** as well as the open-chain tautomers **1a** and **2a** since all of these have many H-donor and acceptor groups. The wealth of possible H-bonding interactions in pterins makes it difficult to ascertain how H-bonding affects the equilibrium, but the general trend observed between K_{eq} and the β_{KT} scale (Figures S3e and S3f) shows solvents that form stronger hydrogen bonds favor the pyran form. While trace water contamination in higher-polarity solvents can be problematic and could affect the equilibrium, no trend was found between the K_{eq} values and water concentration as observed from ^{1}H NMR spectra in each solvent analyzed (Supporting Information, Figure S4). One hydrogen-bonding interaction that may provide a significant stabilization of the pyran forms **1b** and **2b** involves the donation of N−H proton at N8 to basic solvents.

Consideration of possible steric repulsion between H7 and the γ-hydroxyl group in the open chain forms **1a** and **2a** led us to perform DFT geometry optimizations on both structures. These calculations unanimously resulted in a structure (Figure 6, right and Supporting Information, Figure S5) forming an intramolecular hydrogen bond between pterin N5 and the γ-hydroxyl proton made possible through rotation of the pterin group around C6−Cα bond (Figure 6). Optimized H-bonded

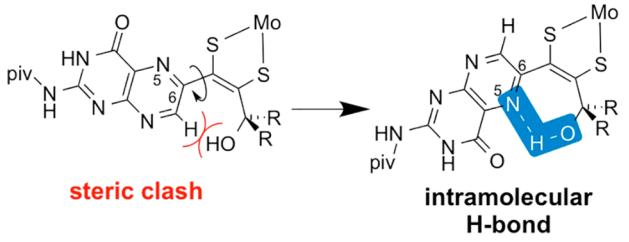

Figure 6. Structures of two possible rotamers of **1a** and **2a**. A steric clash arises when H7 is oriented toward the hydroxyl group in the coplanar conformation of the pterin and dithiolene units. Pterin rotation around the C6−Cα bond produces a more stable conformation due to possible formation of an intramolecular N5···H−O hydrogen bond (highlighted in blue).

structures had dihedral angles between the pterin and dithiolene molecular planes (Figure 7) of 149.6° in the

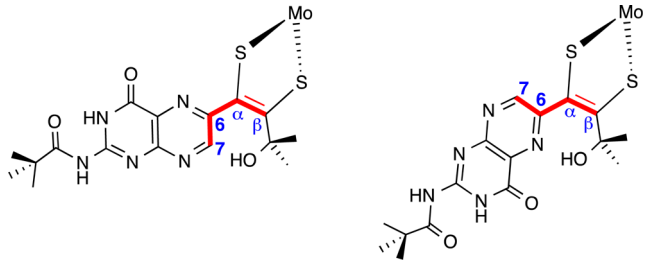

Figure 7. Structures illustrating the dihedral angle C7−C6−Cα−Cβ measured in the theoretical calculations; (left) for coplanar pterin and dithiolene groups, the dihedral angle C7−C6−Cα−Cβ is 0°; (right) for coplanar pterin and dithiolene groups, the dihedral angle C7−C6−Cα−Cβ is 180°.

optimized structure for **1a** and 136.9° for **2a**. This rearrangement to the lower-energy structure in Figure S5 occurs even when the calculation is initiated with H7 adjacent to the hydroxyl group (per Figure 6, left). Such intramolecular hydrogen bonding has been observed as a stabilizing interaction in some systems exhibiting ring−chain tautomerism.[37,41] Rotation of the pterin group in **1a** and **2a** has precedent in studies of $(Et_4N)[Tp^*Mo(O)(S_2BMOQO)]$ previously reported by us in a model structurally similar to **1** and **2,** with a quinoxaline group in place of a pterin. Quinoxaline rotation precedes an intramolecular cyclization process to form a pyrrolo−dithiolene ligand.[42,43]

The geometry optimization results above prompted us to further study the energies of different rotamers of **1a**. The potential energy diagram in Figure 8 was generated from energy calculations as the pterin/dithiolene dihedral angle around the C6−Cα bond (Figure 7) was varied. The diagram in Figure 8 shows that, although limited pterin rotation is energetically reasonable between the dihedral angles of ∼40−320°, the intramolecular hydrogen bond interaction is optimal near 150°, where this is the most stable rotamer of **1a**. Results from 1D NOESY experiments (Supporting Information, Figure S6) of **1** in chloroform-*d* show that **1a** exists in solution primarily as the rotamer depicted at 150°, with a smaller population of the 90° and 270° rotamers shown in Figure 6. When the dihedral angle approaches 0° or 360° placing H7 in close in proximity to the hydroxyl group, the energy increases dramatically to 800 kJ/mol. Such an energy barrier must impede full 360° pterin rotation and restricts the pterin rotational motion to dihedral angles between ∼40−320°. Furthermore, this barrier prevents any conformation where the pterin is near coplanarity with dithiolene, such as is implied by the left structure in Figure 6. We conclude that, in solution, the pterins of **1a** and **2a** are never coplanar with the dithiolene in this fashion.

Thermodynamic Parameters. ΔH, ΔS, and ΔG values for the pyran tautomerism in **1** and **2** were calculated from van't Hoff plots of ^{1}H NMR data collected at varying sample temperatures. Spectra were recorded at 10 °C intervals between 20 and −20 °C, except in DMSO-d_6 where 5 °C intervals were used between 25 and 40 °C. Changing sample temperature caused a convergence of signals in some solvents, which complicated the acquisition of integration data. Hence the calculated thermodynamic parameters (Table 2) were limited to select solvents that did not exhibit signal convergence (DMSO-d_6, DMF-d_7, acetonitrile-d_3, THF-d_8, and chloroform-*d*

DOI: 10.1021/acs.inorgchem.5b00532
Inorg. Chem. 2015, 54, 8214−8222

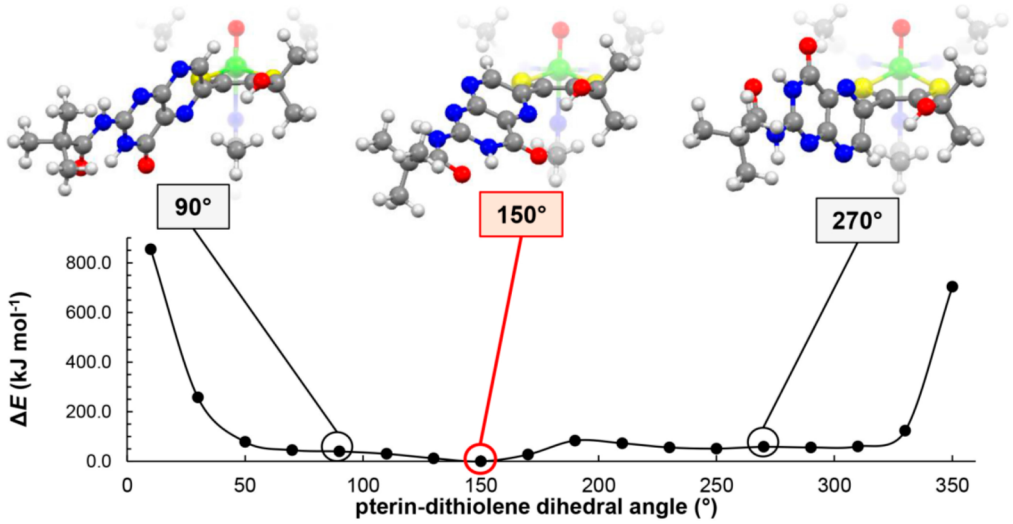

Figure 8. Potential energy diagram of **1a** with various dihedral angles measured between the pterin and dithiolene moieties. Structures of **1a** at select pterin−dithiolene dihedral angles are included above each diagram; the structure best illustrating the N5···H−O hydrogen bond is highlighted in red.

Table 2. Thermodynamic Parameters ΔH (kJ mol^{-1}), ΔS (J mol^{-1} K^{-1}), ΔG, and $\Delta G'^{a}$ (kJ mol^{-1}) for 1 and 2 from van't Hoff Analysis at 25 °C

solvent	ΔH	ΔS	ΔG	$\Delta G'^{a}$
DMSO-d_6	−31.2(7)	−81(2)	−6.98(3)	−6.6(3)
DMF-d_7	−30.8(4)	−80(1)	−6.90(2)	−4.8(2)
acetonitrile-d_3	−28(3)	−73(8)	−6.0(5)	−4.5(3)
THF-d_8	−14(1)	−40(4)	−1.6(1)	−1.2(4)
chloroform-d	−9(2)	−35(9)	1.5(5)	2.2(3)
DMSO-d_6 (**2**)^{b}	−24(2)	−65(7)	−4.9(1)	−5(2)

$^{a}\Delta G'$ values are calculated from K_{eq} constants in Table 1 at 25 °C. ^{b}Parameters for **2** were obtained only in DMSO-d_6 due to convolution of signals in all other solvents.

for **1**; only DMSO-d_6 for **2**). As seen in the van't Hoff plots in Supporting Information, Figures S7 and S8, the pyran form is favored as the sample temperature decreases in all solvents analyzed, which is expected based on several studies of systems exhibiting ring−chain equilibria.[26,27] The ΔG values for **1** in Table 2 are close to those values ($\Delta G'$) calculated from the equation $\Delta G' = -RT \ln(K_{eq})$ at 25 °C using the K_{eq} constants in Table 1, with the exception of data from DMF-d_7 and acetonitrile-d_3.

The ΔG values are negative in all solvents except chloroform-d, signifying that pyran cyclization is thermodynamically favored and spontaneous in the polar solvents. This matches the K_{eq} data in Table 1 where the pyran tautomer is favored in THF-d_8, acetonitrile-d_3, DMF-d_7, and DMSO-d_6, whereas the open species is favored in chloroform-d. The values of ΔH are negative in all solvents, even for chloroform that has a positive free energy value. The negative enthalpy values are unsurprising since pyran cyclization involves the formation of two new bonds: C7−O (to close the pyran ring) and N8−H. All ΔS values are negative, which is also expected since conversion of the open species to the pyran form inhibits fluxional motion of the pterin moiety via the C6−Cα bond as well as free rotation of the other dithiolene substituent −CR$_2$OH (R = Me in **1**, Et in **2**), via the Cβ−Cγ bond. It is important to note that all free energy values in Table 2 are small in magnitude, spanning a range of ∼8.5 kJ mol^{-1} between the two extreme solvents DMSO and chloroform for **1**. In the context of Moco, the small nature of these free energies signifies that pyran scission and cyclization are energetically inexpensive, making the interconversion between both forms an energetically facile process. Interestingly, all thermodynamic values become more negative in **1** as solvent polarity increases. The formation of stronger intermolecular associations, such as hydrogen bonds, between solvent molecules and **1** may be a possible explanation for the increasingly negative enthalpy values. More negative entropy terms corroborate this hypothesis because association of solvent molecules solvating **1** in a restricted, more ordered arrangement would decrease the entropy of the system.

During the present study, attempts were made to observe changes in the Mo electronic environment due to pyran cyclization and scission in **1** and **2** using cyclic voltammetry (CV) and solution FT-IR. Unfortunately, results from these analyses were inconclusive due to difficulties posed by the techniques themselves. Electrolyte required for the CV experiment increases the solvent dielectric and thus favors the pyran cyclization state of **1** and **2** in solution. Comparison of vibrational frequencies in different solvents using FT-IR is complicated by overlapping solvent vibrational modes.

DISCUSSION

Several hypotheses in the literature offer speculations on the catalytic role played by the pyranopterin−dithiolene ligand of the molybdenum cofactor (Moco). One idea suggests that reversible pyran ring formation in Moco could be involved in Mo redox tuning.[6,14,44−46] Here we present the first experimental results from a Mo-pterin−dithiolene model in support of a feasible, low-energy dynamic cyclization process. This report provides a detailed investigation of reversible pyran ring scission and cyclization in two pyranopterin dithiolene models for Moco.

Reversible pyranopterin cyclization may be considered a complicated example of the simpler and much-studied organic transformation known as ring−chain tautomerism, exemplified in Figure 9. Ring−chain tautomers exhibit a preference for one tautomer under certain conditions. Most commonly the cyclized ring form predominates in low-polarity solvents, while the open, chain structure is favored in higher-polarity

DOI: 10.1021/acs.inorgchem.5b00532
Inorg. Chem. 2015, 54, 8214−8222

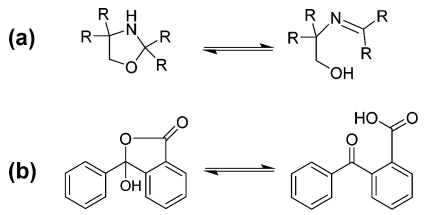

Figure 9. Examples of ring−chain tautomerism in (a) oxazolidines[32] and (b) *o*-benzoylbenzoic acids.[38]

solvents. Hydrogen bonding of solvents can also influence the tautomer equilibrium.

The Moco model complexes in this study also exhibit a solvent-dependent behavior that determines whether the cyclized, pyranopterin form predominates versus the cleaved, open-chain pterin form (Figure 2). The models **1** and **2** exhibit the ring form (the pyranopterin form) in high-polarity solvents, while the chain form, (the open pterin−dithiolene) predominates in low-polarity solvents. Though the behavior of the models differs from the majority of ring−chain tautomers, it is a behavior that has precedence in certain organic ring−chain tautomer systems.[38−40] A computational analysis done on our model complexes **1** and **2** revealed that a reason for the preference of the open-chain pterin−dithiolene form in low-polarity solvent is likely a result of a rotation of the pterin producing a lower-energy structure having an intramolecular hydrogen bond (Figure 7). The computational study included calculation of total energy as a function of pterin rotation required to attain the intramolecular hydrogen bond (Figure 8). The energy profile shows that coplanarity of pterin and dithiolene groups is energetically impossible and that pterin motion is energetically restricted to dihedral angles of 40−320° between the pterin and dithiolene planes. Thermodynamic parameters obtained from variable-temperature ^{1}H NMR experiments confirm that the free energy difference between the pyranopterin and open-chain pterin forms is small (<10 kJ/mol).

Currently, the only protein crystal structures definitively exhibiting Moco in the open, bicyclic form are of nitrate reductase (NR) from *Escherichia coli* (1Q16)[17] and ethylbenzene dehydrogenase (EBDH) from *Aromatoleum aromaticum* (2IVF).[18] As these enzymes are members of the DMSO reductase family, their active sites consist of a bis-MPT-containing Moco, with one MPT in the pyranopterin form and one MPT in an open pterin−dithiolene structure (Figure 10).

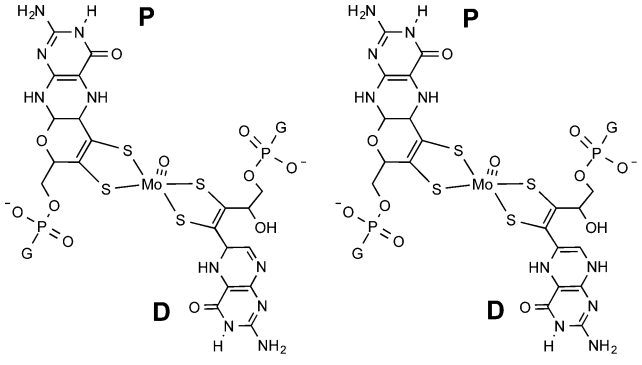

Figure 10. Structure of Moco in NR (left) and EBDH (right), where the proximal (P) pterin dithiolene is in the pyran form, while the distal (D) one is in the open form. G = guanine mononucleotide.

In both crystal structures, the MPT proximal to the [4Fe−4S] cluster (P in Figure 10) is in the pyranopterin form, while the distal MPT ligand (D in Figure 10) is observed in an uncyclized, open form. The proximal MPT is presumed to be involved in electron transport between the [4Fe−4S] cluster and Mo, whereas the distal MPT has been suggested to modulate Mo oxidation state through pyran cyclization dynamics.[6] Both the NR and EBDH structures show a stabilizing interaction of the open-chain forms involving multiple H-bonds between protein residues and the −OH group.[47] Low-polarity groups around the pyran ring of the cyclized forms indicate that the protein environment is being used to selectively stabilize one form. The reported structures of NR and EBDH (Figure 10) show different dihydropterin tautomers for the uncyclized distal pterin dithiolene, though it must be noted that the electron density maps for EBDH were reported as insufficient for determination of the precise pterin structure.[18]

The results from our work confirm that the proposed reversible pyran scission and cyclization in Mo enzymes is possible. The small energies involved in the tautomerism of our model suggest similar energetically inexpensive costs associated with interconversion of pyran and open-chain forms of the pterin−dithiolene in the enzymes that could be compensated by H-bond formation. The results are also consistent with the notion that pyran cyclization dynamics in the active sites of Mo and W enzymes will be controlled in part by local polarities established by neighboring active site residues. The apparent polarity around the pyranopterin and open pterin regions in the enzymes is opposite of that observed in our solubilized model, but a direct comparison of the model to the enzymes is complicated since the model system has considerable flexibility, while the pterin−dithiolene in MPT is tightly constrained by multiple H-bonds.

It is anticipated that the electronic environment at Mo in **1** and **2** will change with pyran cyclization and scission. In the X-ray crystal structure[22] of **1** in the pyranopterin−dithiolene form, the pyran ring formation locks the pterin into a conformation where the pyrazine and dithiolene are nearly coplanar (dihedral angle ≈ 7°), allowing electronic communication between the Mo atom, the dithiolene, and pterin moieties. However, in the chain or open form, steric repulsion between the −OH and the pterin H7 causes the pterin to rotate out of coplanarity, thus electronically isolating the dithiolene from the pterin group. Similar changes in planarity between pterin and dithiolene groups within Moco could be a mechanism to control the electronic structure in the catalytic reaction.

Further investigation may reveal how pyran ring−chain tautomerism changes the electronic structure in **1** and **2**. Here we note that, in addition to pyran scission and cyclization, the Mo reduction potential may be controlled by other pterin modifications, such as protonation or changing the pterin oxidation state, and these may be coupled to pyran cyclization dynamics to significantly affect the Mo reduction potential. Protonation and chemical reduction of models **1** and **2** may provide more information regarding this behavior, and these studies are currently underway in our lab.

CONCLUSIONS

In this study we have reported K_{eq} and thermodynamic constants for the solvent-dependent tautomerism between the pyran and open forms of pterin−dithiolene complexes **1** and **2**. These values show that the pyran form is more favored in polar

DOI: 10.1021/acs.inorgchem.5b00532
Inorg. Chem. 2015, 54, 8214−8222

solvents and point to a strong correlation with solvent dielectric constant. Polar solvents may stabilize the closed form either through stabilization of a charged intermediate, formation of intermolecular hydrogen bonds, or some combination of both. Stabilization of the open form in less polar solvents is likely to occur by an intramolecular N···H−O hydrogen bond between the hydroxyl group and the pyrazine N5 as predicted by DFT geometry optimization calculations. These K_{eq} trends may offer insight into the mechanism of reversible pyran scission and cyclization in Mo enzymes.

■ ASSOCIATED CONTENT

Supporting Information

Assignments of pertinent ^{1}H NMR spectral regions in all solvents analyzed; plots of equilibrium and thermodynamic constants versus measures of solvent polarity; plots of H_2O data from ^{1}H NMR spectra versus K_{eq}; 1D NOESY spectrum of **1a**; van't Hoff plots for **1** and **2**; geometry optimization structures of **1a** and **2a**. This material is available free of charge via the Internet at http://pubs.acs.org.

■ AUTHOR INFORMATION

Corresponding Author

*E-mail: sburgmay@brynmawr.edu.

Funding

The authors wish to acknowledge the NIH (GM081848) and the NSF (CHE-0958996) for financial assistance.

Notes

The authors declare no competing financial interest.

■ REFERENCES

(1) Rajagopalan, K. V. Biochemistry of the Molybdenum Cofactors. In *Molybdenum Enzymes, Cofactors and Model Systems;* ACS Symposium Series Vol. *535*; American Chemical Society: Washington, DC, 1993; pp 38−49.

(2) Leimkühler, S.; Wuebbens, M. M.; Rajagopalan, K. V. *Coord. Chem. Rev.* **2011**, *255*, 1129−1144.

(3) Johnson, J. L.; Hainline, B. E.; Rajagopalan, K. V.; Arison, B. H. *J. Biol. Chem.* **1984**, *259*, 5414−5422.

(4) Fischer, B.; Enemark, J. H.; Basu, P. *J. Inorg. Biochem.* **1998**, *72*, 13−21.

(5) Basu, P.; Burgmayer, S. J. N. *Coord. Chem. Rev.* **2011**, *255*, 1016−1038.

(6) Rothery, R. A.; Stein, B.; Solomonson, M.; Kirk, M. L.; Weiner, J. H. *Proc. Natl. Acad. Sci. U.S.A.* **2012**, *109*, 14773−14778.

(7) Pateman, J. A.; Cove, D. J.; Rever, B. M.; Roberts, D. B. *Nature* **1964**, *201*, 58−60.

(8) Raghavan, R.; Dryhurst, G. *J. Electroanal. Chem. Interfacial Electrochem.* **1981**, *129*, 189−212.

(9) Ege-Serpkenci, D.; Dryhurst, G. *Bioelectrochem. Bioenerg.* **1982**, *9*, 175−195.

(10) Karber, L. G.; Dryhurst, G. *J. Electroanal. Chem. Interfacial Electrochem.* **1982**, *136*, 217−289.

(11) Ege-Serpkenci, D.; Raghavan, R.; Dryhurst, G. *Bioelectrochem. Bioenerg.* **1983**, *10*, 357−376.

(12) Karber, L. G.; Dryhurst, G. *J. Electroanal. Chem. Interfacial Electrochem.* **1984**, *160*, 141−157.

(13) Diculescu, V. C.; Militaru, A.; Shah, A.; Qureshi, R.; Dryhurst, G. *J. Electroanal. Chem. Interfacial Electrochem.* **2010**, *647*, 1−7.

(14) Enemark, J. H.; Garner, C. D. *J. Biol. Inorg. Chem.* **1997**, *2*, 817−822.

(15) Soyka, R.; Pfleiderer, W.; Prewo, R. *Helv. Chim. Acta.* **1990**, *73*, 808−826.

(16) Soyka, R.; Pfleiderer, W. *Pteridines* **1990**, *2*, 63−74.

(17) Bertero, M. G.; Rothery, R. A.; Palak, M.; Hou, C.; Lim, D.; Blasco, F.; Weiner, J. H.; Strynadka, N. C. J. *Nat. Struct. Biol.* **2003**, *10*, 681−687.

(18) Kloer, D. P.; Hagel, C.; Heider, J.; Schulz, G. E. *Structure* **2006**, *14*, 1377−1388.

(19) Bradshaw, B.; Dinsmore, A.; Collison, D.; Garner, C. D.; Joule, J. A. *J. Chem. Soc., Perkin Trans.* **2001**, 3232−3238.

(20) Bradshaw, B.; Collison, D.; Garner, C. D.; Joule, J. A. *Chem. Commun.* **2001**, 123−124.

(21) Burgmayer, S. J. N.; Pearsall, D. L.; Blaney, S. M.; Moore, E. M.; Sauk-Schubert, C. *J. Biol. Inorg. Chem.* **2004**, *9*, 59−66.

(22) Williams, B. R.; Fu, Y.; Yap, G. P. A.; Burgmayer, S. J. N. *J. Am. Chem. Soc.* **2012**, *134*, 19584−19587.

(23) Burgmayer, S. J. N.; Kim, M.; Petit, R.; Rothkopf, A.; Kim, A.; Bel Hamdounia, S.; Hou, Y.; Somogyi, A.; Habel-Rodriguez, D.; Williams, A.; Kirk, M. L. *J. Inorg. Biochem.* **2007**, *101*, 1601−1616.

(24) Frisch, M. J.; Trucks, G. W.; Schlegel, H. B.; Scuseria, G. E.; Robb, M. A.; Cheeseman, J. R.; Scalmani, G.; Barone, V.; Mennucci, B.; Petersson, G. A.; Nakatsuji, H.; Caricato, M.; Li, X.; Hratchian, H. P.; Izmaylov, A. F.; Bloino, J.; Zheng, G.; Sonnenberg, J. L.; Hada, M.; Ehara, M.; Toyota, K.; Fukuda, F.; Hasegawa, J.; Ishida, M.; Nakajima, T.; Honda, Y.; Kitao, O.; Nakai, H.; Vreven, T.; Montgomery, J. A., Jr.; Peralta, J. E.; Ogliaro, F.; Bearpark, M.; Heyd, J. J.; Brothers, E.; Kudin, K. N.; Staroverov, V. N.; Kobayashi, R.; Normand, J.; Raghavachari, K.; Rendell, A.; Burant, J. C.; Iyengar, S. S.; Tomasi, J.; Cossi, M.; Rega, N.; Millam, M. J.; Klene, M.; Knox, J. E.; Cross, J. B.; Bakken, V.; Adamo, C.; Jaramillo, J.; Gomperts, R.; Stratmann, R. E.; Yazyev, O.; Austin, A. J.; Cammi, R.; Pomelli, C.; Ochterski, J. W.; Martin, R. L.; Morokuma, K.; Zakrzewski, V. G.; Voth, G. A.; Salvador, P.; Dannenberg, J. J.; Dapprich, S.; Daniels, A. D.; Farkas, Ö.; Foresman, J. B.; Ortiz, J. V.; Cioslowski, J.; Fox, D. J. *Gaussian 09,* Revision C.01; Gaussian, Inc.: Wallingford, CT, 2009.

(25) Bowden, K.; Byrne, J. M. *J. Chem. Soc., Perkin Trans. 2* **1997**, *1*, 123−127.

(26) Valters, R. E.; Flitsch, W. *Ring-Chain Tautomerism;* Katritzky, A. R., Ed.; Plenum Press: New York, 1985; p 169.

(27) Escale, R.; Verducci, J. *Bull. Soc. Chim.* **1974**, 1203−1206.

(28) Santamaria-Araujo, J. A.; Wray, V.; Schwarz, G. *J. Biol. Inorg. Chem.* **2012**, *17*, 113−122.

(29) Clinch, K.; Watt, D. K.; Dixon, R. A.; Baars, S. M.; Gainsford, G. J.; Tiwari, A.; Schwarz, G.; Saotome, Y.; Storek, M.; Belaidi, A. A.; Santamaria-Araujo, J. A. *J. Med. Chem.* **2013**, *56*, 1730−1738.

(30) Kosower, E. M. *J. Am. Chem. Soc.* **1958**, *80*, 3253−3260.

(31) Kamlet, M. J.; Taft, R. W. *J. Am. Chem. Soc.* **1976**, *98*, 377−383.

(32) Sandström, M.; Persson, I.; Persson, P. *Acta Chem. Scand.* **1990**, *44*, 653−675.

(33) Paukstelis, J. V.; Hammaker, R. M. *Tetrahedron Lett.* **1968**, 3557−3560.

(34) Dorman, L. C. *J. Org. Chem.* **1967**, *32*, 255−260.

(35) Potekhin, A. A.; Zhdanov, S. L.; Gindin, V. A.; Ogloblin, K. A. *Zh. Org. Khim.* **1976**, *12*, 2090−2094.

(36) Whitting, J. E.; Edward, J. T. *Can. J. Chem.* **1971**, *49*, 3799−3806.

(37) McDonagh, A. F.; Smith, H. E. *J. Org. Chem.* **1968**, *33*, 1−8.

(38) Bhatt, M. V.; Kamath, K. M. *J. Chem. Soc. B* **1968**, 1036−1044.

(39) Bhatt, M. V.; Kamath, K. M. *Tetrahedron Lett.* **1966**, 3885−3890.

(40) Walter, W.; Rohloff, C. *Justus Liebigs Ann. Chem.* **1977**, 485−490.

(41) McDonagh, A. F.; Smith, H. E. *Chem. Commun.* **1966**, 374.

(42) Matz, K. G.; Mtei, R. P.; Leung, B.; Burgmayer, S. J. N.; Kirk, M. L. *J. Am. Chem. Soc.* **2010**, *132*, 7830−7831.

(43) Matz, K. G.; Mtei, R. P.; Rothstein, R.; Kirk, M. L.; Burgmayer, S. J. N. *Inorg. Chem.* **2011**, *50*, 9804−9815.

(44) Jacques, J. G. J.; Fourmond, V.; Arnoux, P.; Sabaty, M.; Etienne, E.; Grosse, S.; Baiso, F.; Bertrand, P.; Pignol, D.; Léger, C.; Guigliarelli, B.; Burlat, B. *Biochim. Biophys. Acta* **2014**, *1837*, 277−286.

(45) Aguey-Zinsou, K. F.; Bernhardt, P. V.; Leimkühler, S. *J. Am. Chem. Soc.* **2003**, *125*, 15352−15358.

DOI: 10.1021/acs.inorgchem.5b00532
Inorg. Chem. 2015, 54, 8214−8222

(46) McNamara, J. P.; Joule, J. A.; Hillier, I. H.; Garner, C. D. *Chem. Commun.* **2005**, 177−179.
(47) Rothery, R. A.; Weiner, J. H. *J. Biol. Inorg. Chem.* **2015**, *20*, 349−372.

DOI: 10.1021/acs.inorgchem.5b00532
Inorg. Chem. 2015, 54, 8214−8222